Droplet impact on deep liquid pools: Rayleigh jet to formation of secondary droplets

Eduardo Castillo-Orozco,* Ashkan Davanlou,* Pretam K. Choudhury, and Ranganathan Kumar†
Department of Mechanical and Aerospace Engineering, University of Central Florida, Orlando, Florida 32816, USA
(Received 1 September 2015; revised manuscript received 2 November 2015; published 30 November 2015)

The impact of droplets on a deep pool has applications in cleaning up oil spills, spray cooling, painting, inkjet printing, and forensic analysis, relying on the changes in properties such as viscosity, interfacial tension, and density. Despite the exhaustive research on different aspects of droplet impact, it is not clear how liquid properties can affect the instabilities leading to Rayleigh jet breakup and number of daughter drops formed after its pinch-off. In this article, through systematic experiments we investigate the droplet impact phenomena by varying viscosity and surface tension of liquids as well as impact speeds. Further, using numerical simulations, we show that Rayleigh-Plateau instability is influenced by these parameters, and capillary time scale is the appropriate scale to normalize the breakup time. Based on Ohnesorge number (Oh) and impact Weber number (We), a regime map for no breakup, Rayleigh jet breakup, and crown splash is suggested. Interestingly, crown splash is observed to occur at all Ohnesorge numbers; however, at high Oh, a large portion of kinetic energy is dissipated, and thus the Rayleigh jet is suppressed regardless of high impact velocity. The normalized required time for the Rayleigh jet to reach its peak varies linearly with the critical height of the jet.

DOI: 10.1103/PhysRevE.92.053022 PACS number(s): 47.55.df, 47.20.Gv

I. INTRODUCTION

The study of droplet impact phenomena can benefit in many applications such as oil spills [1–4], spray cooling and painting [5], inkjet printing [6], agricultural [7,8], droplet manipulation [9–11], internal combustion engines [12], and even forensic bloodstain pattern analysis [13]. The impact studies can be classified according to the type of target surface such as dry solid surface [14–17], thin liquid film [17,18], and deep liquid pool [19,20]. In these studies, spreading, splashing, bouncing, crater depth, crown formation, cavity evolution, and bubble entrainment were visualized on any of the above-mentioned target surfaces and studied in detail. Full coalescence where the droplet fully merges with the interface was identified and a more complex phenomenon of partial coalescence, where the merging is not as yet complete, was studied [21–23].

The focus of this paper is the Rayleigh jet pinch-off and formation of secondary drops; therefore the Ohnesorge number (ratio of viscosity to surface tension force, $\mathrm{Oh} = \mu/\sqrt{\sigma\rho R}$), is an appropriate parameter to describe the interfacial liquid-liquid interactions [24,25]. The Weber number (inertia to surface tension force $\mathrm{We} = \rho U^2 R/\sigma$) and Reynolds number (ratio of inertia to viscous force, $\mathrm{Re} = \rho U R/\mu$)) are used to describe the crown splash, where μ, σ, and ρ are the dynamic viscosity, surface tension, and density of the liquids; R is the initial droplet radius; and U is the impact velocity. Weber number incorporates the effect of droplet velocity (releasing height). It is suggested that the role of gravity is the most important before the rupture [26,27]. Since gravity is incorporated indirectly in these parameters through droplet velocity, Bond number (effect of gravity vs surface tension force, $\mathrm{Bo} = \Delta\rho g R^2/\sigma$) is not used to plot the results in the current study. However, the effect of drop size, surface tension, and density (key parameters in Bond number) are either studied separately or captured through other nondimensional numbers (i.e., Oh and We). Thus, the Ohnesorge number, Weber number, and Reynolds number are the main parameters that play a strong role in determining the dynamics of instability on the liquid surface due to droplet impact.

Despite this knowledge, results for a wide range of these parameters are not generally available. For example, since the effect of impact velocity was not considered in [21], pinch-off was thought of as the only mechanism for the early dynamics of coalescence. The liquid drops were deposited gently onto the surface so that the kinetic energy was low. Because of this low kinetic energy, the coalescence process terminates when either the droplet or the pinched region submerges into the reservoir. Therefore, there is no rebound occurring which would result in jet formation. Thoroddsen and Takehara suggested that the surface tension time scale can be used to scale the time associated with partial coalescence and that the cascade of a drop is limited due to viscous effects [28]. Hoepffner and Paré showed that the vortex rings created by viscous shear in the jet could delay the pinch-off and recoil as a liquid filament [29]. Walls *et al.* focused on the special case when both gravitational and viscous effects are important in jet-drop formation as in sea slicks and metalworking fluid [30]. In their work, air is injected into the bottom of a water-glycerol solution. Ghabache *et al.* [31] also investigated the jet produced by bubble bursting, focusing on the influence of viscosity and gravity. They correlated the initial shape and aspect ratio of the cavity to the height and thickness of the jet in bubble bursting. Deegan *et al.* looked into the distinct dynamical origins of the secondary droplets [32]. They developed a regime map based on We and Re for crown splash (instability in Peregrine sheet that leads to large droplets) and found a power law relationship between those two numbers.

Additional studies on jet breakup have been conducted to understand the effects of drop size, interfacial tension, and viscosity [33–35]. Numerical studies such as the volume of fluid (VOF) were applied effectively to track free boundaries or fluid-fluid interfaces or predict the instabilities, splashing lamella, and cusp formation [36,37]. Regime maps have been developed for vortex ring formation, bubble entrapment, and

*These authors contributed equally to this work.
†Corresponding author: ranganathan.kumar@ucf.edu

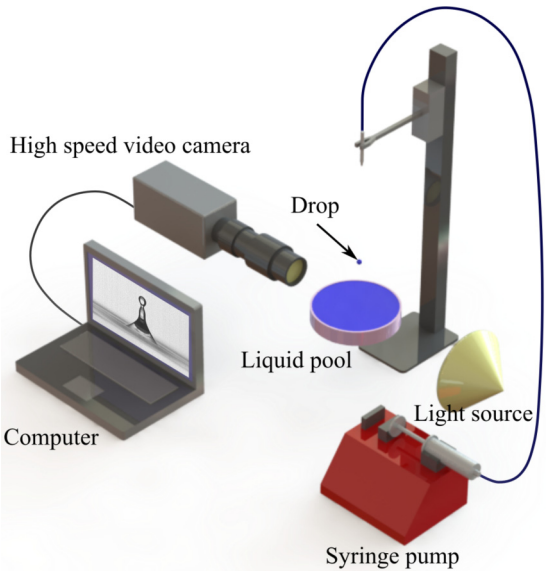

FIG. 1. (Color online) Experimental setup.

jet formation based on Weber number, Froude number, or capillary number [19,38]; however, not all regimes were captured due to the limited range of these parameters.

The primary objective of this paper is to investigate the influence of physicochemical properties of the fluids and impact velocity on Rayleigh jet, pinch-off of the secondary (daughter) drop, and the crown formation. In this regard, the release height of the droplet is varied to generate a range of impact velocities, with the Weber number extending to 1400. In order to systematically study the influence of fluid properties such as viscosity, surface tension, and density, a wide range of fluids is tested, resulting in Ohnesorge numbers in the range 0.0033–0.136. These experiments were complemented by axisymmetric simulations based on VOF and continuum surface force (CSF) methods. The combination of experimental and numerical studies was used to determine the critical Weber number at which the jet pinches off and secondary droplet formation occurs. These models were not only validated by the experiments, but they also served the role of understanding the Rayleigh-Plateau instability in jet breakup through the pressure and velocity distribution at the neck during stretching of the Rayleigh jet.

II. EXPERIMENTAL SETUP

Figure 1 shows the schematic of the experimental setup. A circular transparent petri dish with a diameter of 80 mm and thickness of 13 mm was used as the container. The container was large enough to minimize the wall effect. Drops were generated using a syringe pump (World Precision Instruments) at a flow rate of 100 μl/min, using a needle with a nominal outer diameter of 0.64 mm. A high-speed camera (i-Speed 2, Olympus) connected to a zoom lens (Navitar) captured the events at 2000 frames per second with a resolution of 576 × 432 pixels. The images were extracted from the videos and analyzed using MATLAB. The uncertainty of the measurements from the imaging was 0.126 mm. The illumination was provided by a 1000-W halogen lamp. The camera was set to capture the interface and droplet from the side. The heat generation caused by illumination was controlled to avoid thermal gradient between the two media. The properties of different liquids along with the droplet diameter, D_o, used in the experiment are presented in Table I. All the experiments were carried out at room temperature of 24.6 °C ± 1 °C, and were repeated at least three times to assure repeatability of the data.

Droplets were generated using a syringe pump, needle, and plastic tubing. The release height was controlled using a one-dimensional (1D) stage which had micrometer size precision. The size of droplets was consistent for a given fluid as the gravitational force overcomes the capillary force. After each test, the syringe, tubing, and container were changed.

III. NUMERICAL APPROACH

A. Numerical model and governing equations

The volume of fluid method (VOF) [39] was used in combination with the continuum surface force (CSF) [40] model and implemented in the open-source platform, OPENFOAM. The flow conditions caused by the drop impact on a liquid surface were considered to be laminar and axisymmetric. This method considers two different phases as one fluid in the entire domain, where the phases within the domain are tracked by variable γ that is based on the volume fraction. The volume fraction takes on values between 0 and 1. Then the physical properties are defined using volume fraction as $\rho = \gamma\rho_l + (1-\gamma)\rho_g$, and $\mu = \gamma\mu_l + (1-\gamma)\mu_g$, where ρ_g,

TABLE I. Properties of the tested fluids at room temperature.

Liquids	D_o (mm)	μ (cSt)	ρ(g/cm^3)	σ (mN/m)	Oh
Water	2.50	1.0	1.0	72.0	0.0033
Potassium hydroxide	2.70	1.05	1.0	72.1	0.0033
Ethanol	1.93	1.4	0.79	22.0	0.0085
Ethylene glycol	2.20	17.8	1.1	47.7	0.0815
Silicone oil 5 cSt	1.80	5.0	0.91	19.7	0.0360
Silicone oil 10 cSt	1.80	10.0	0.93	20.1	0.0716
Silicone oil 13 cSt	1.90	13.0	0.94	20.2	0.0907
Silicone oil 14 cSt	1.90	14.0	0.94	20.3	0.0952
Silicone oil 16 cSt	1.96	16.0	0.94	20.4	0.1087
Silicone oil 18 cSt	1.98	18.0	0.95	20.5	0.1222
Silicone oil 20 cSt	2.0	20.0	0.95	20.6	0.1358

μ_g are the density and viscosity of the gaseous phase, and ρ_l, μ_l represent the density and viscosity of the liquid phase. In the gaseous phase, $\gamma = 0$, and in the liquid phase, $\gamma = 1$. At the interface, γ takes on values between 0 and 1, and the weighted values are used. The physical properties such as density and viscosity are considered constant within each phase, but they vary at the gas-liquid interface. The CSF model is used to evaluate the surface tension force in the momentum equation. An artificial convective term or compression term $\nabla \cdot (\boldsymbol{V_r}\gamma[1-\gamma])$ is included in the phase fraction equation, to keep the sharp resolution of the interface [41]. This artificial or compression term is presented only at the interface.

Equations governing the fluid mechanics are the incompressible continuity, momentum, and transport of the volume fraction, which are shown as follows:

$$\nabla \cdot (\rho \boldsymbol{V}) = 0, \tag{1}$$

$$\frac{\partial(\rho \boldsymbol{V})}{\partial t} + \rho(\boldsymbol{V}\cdot\nabla)\boldsymbol{V} = -\nabla p + \nabla\cdot(\mu[\nabla \boldsymbol{V} + (\nabla \boldsymbol{V})^T]) + \rho \boldsymbol{g} + \boldsymbol{F}_\sigma, \tag{2}$$

$$\frac{\partial(\rho\gamma)}{\partial t} + \nabla\cdot(\boldsymbol{V}\gamma) + \nabla\cdot(\boldsymbol{V_r}\gamma[1-\gamma]) = 0, \tag{3}$$

where the velocity field, density, time, pressure, viscosity, and gravity are denoted by $\boldsymbol{V}$, ρ, t, p, μ, and $\boldsymbol{g}$, respectively. $\boldsymbol{F}_\sigma$ is the surface tension force that is taken into account in the momentum equation. $\boldsymbol{V_r}$ is the relative velocity at the interface and it was defined by Weller [41] in Eq. (4):

$$\boldsymbol{V_r} = n_f \min[c_f|\boldsymbol{V}|,\ \max(|\boldsymbol{V}|)]\frac{\nabla\gamma}{|\nabla\gamma|}, \tag{4}$$

where n_f is the unit normal flux on a cell face at the interface region, c_f is the compression constant, and $|\boldsymbol{V}|$ is obtained by the pressure-velocity coupling algorithm. The surface tension force is defined by Eq. (5) and the interfacial curvature is expressed by the CSF model as Eq. (6).

$$\boldsymbol{F}_\sigma = \sigma k \nabla\gamma, \tag{5}$$

$$k = -\nabla\cdot\left(\frac{\nabla\gamma}{|\nabla\gamma|}\right), \tag{6}$$

where the interfacial tension between phases is σ, and the interfacial curvature k. The term $\nabla\gamma$ acts only at the gas-liquid interface, where volume fraction changes.

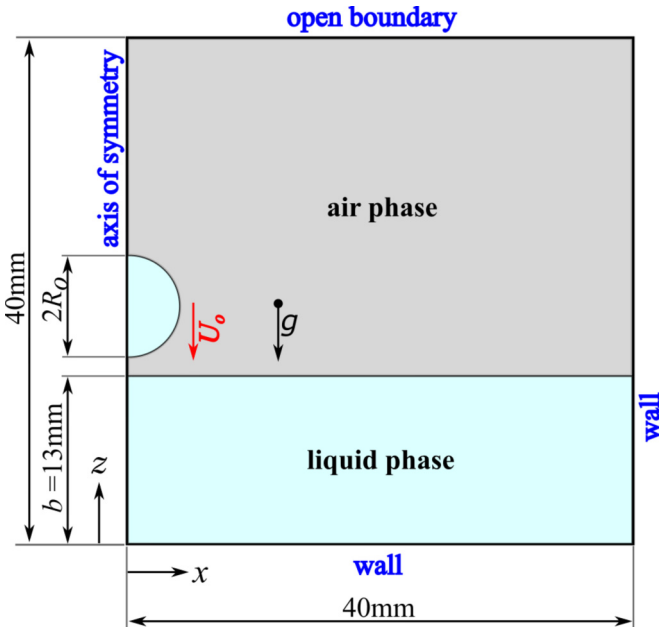

FIG. 2. (Color online) Computational domain and boundary conditions.

B. Initial and boundary conditions

As mentioned earlier, drop impact followed by secondary drop formation was assumed to be axisymmetric. Note that droplet and liquid pool are both the same liquid and are surrounded by air. The droplet domain is shown in Fig. 2. The z axis accounts for the symmetry axis in which the gravity force acts. The bottom and right boundaries are walls with no-slip condition, while the top boundary is an open boundary where

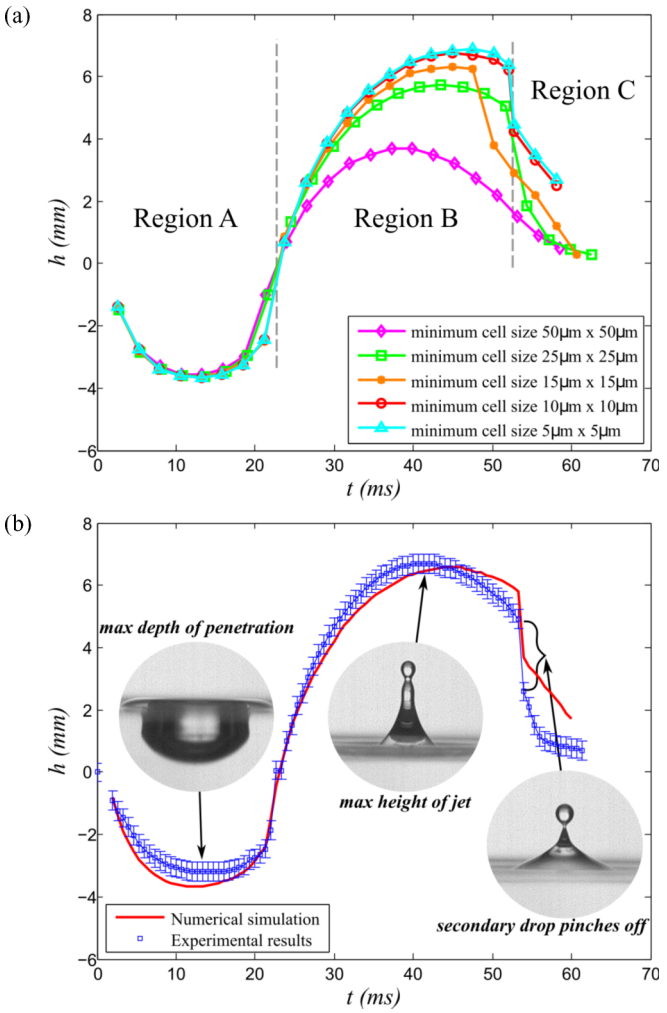

FIG. 3. (Color online) (a) Grid convergence study based on the variation of the height of the cylindrical column for a silicone oil 5 cSt droplet, 1.8 mm diameter, impact on a liquid pool (Re = 324, We = 135, and Oh = 0.036). (b) Quantitative comparison of the numerical results with experiments.

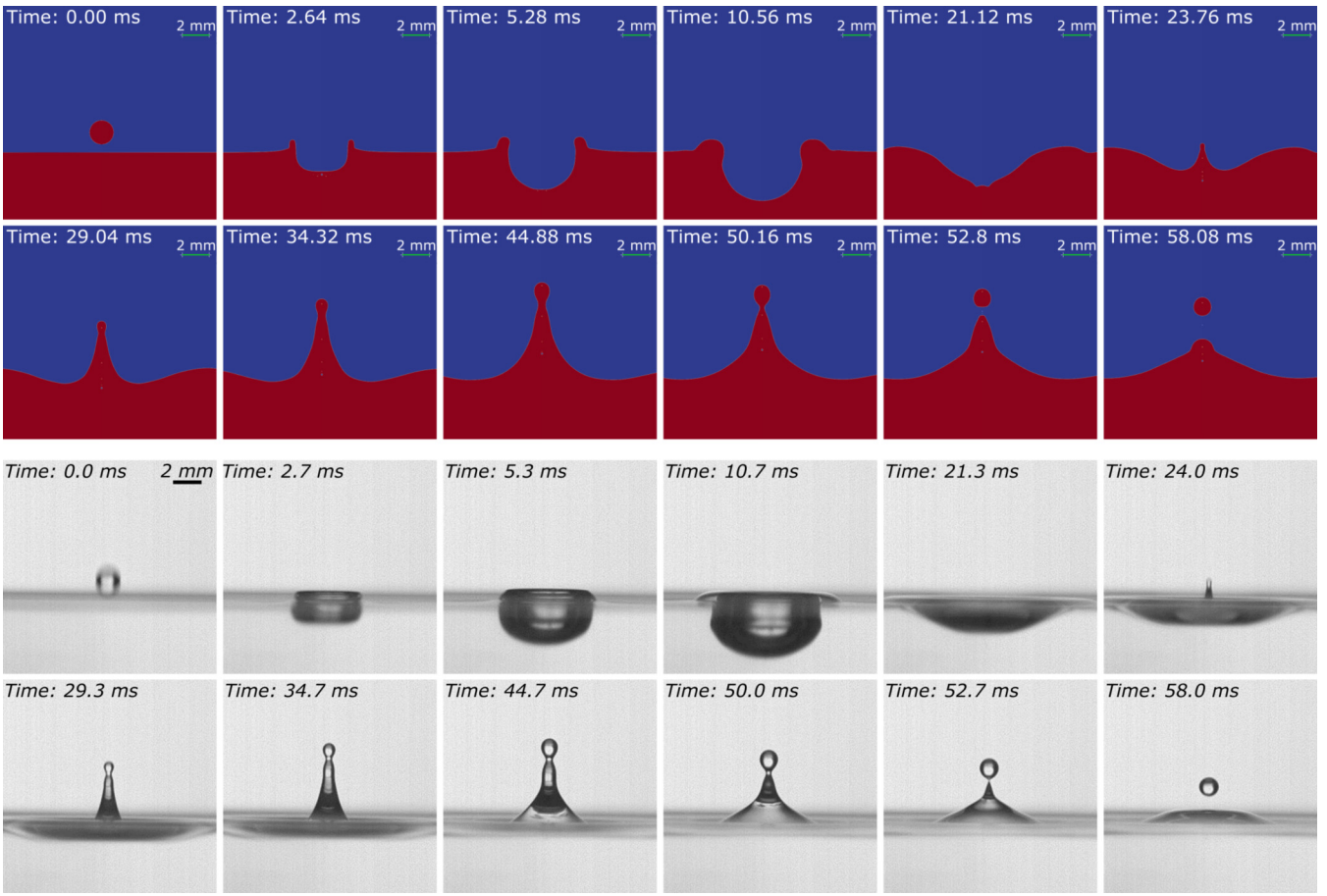

FIG. 4. (Color online) Qualitative comparison of the numerical and experimental results. Time evolution of the Rayleigh jet for the impact of a silicone 5 cSt droplet with its own pool (Re = 324, We = 135, Oh = 0.036).

fluids can flow freely. The domain size is 40 mm × 40 mm. In the beginning of the simulation, the drop and liquid pool are set within the domain by establishing an initial volume fraction. The initial volume fractions in the two phases are air: $\gamma = 0$; liquid: $\gamma = 1$. The capillary pressure difference across the drop interface was considered as the initial condition. In addition, the static pressure was offset by the hydrostatic pressure $\rho g z$ so that the initial pressure at the walls is 0.

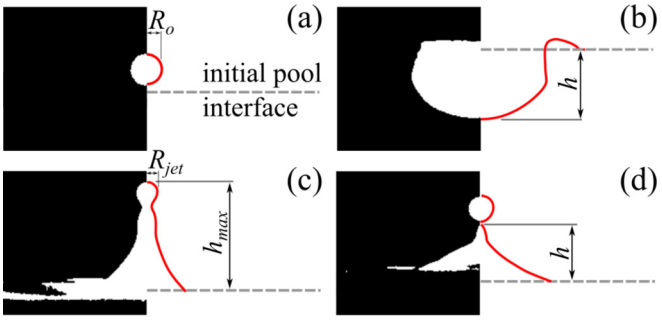

FIG. 5. (Color online) Binary images used for image processing. Sequence of stages of a silicone oil 5 cSt droplet (We = 135, Oh = 0.036). (a) Droplet 0.5 ms before impact upon liquid pool, (b) maximum depth of crater, (c) maximum height of Rayleigh jet, and (d) pinch-off of the secondary droplet.

C. Grid independence

A standard mesh size of 0.16 mm × 0.16 mm was used to create the entire domain, except near the liquid interface where the mesh was refined. Five different mesh types were tested to check for grid independence. The cell sizes used within the refined region were 50 μm × 50 μm, 25 μm × 25 μm, 15 μm × 15 μm, 10 μm × 10 μm, and 5 μm × 5 μm.

The numerical simulation of silicone oil 5 cSt was used to investigate the grid dependence of the solution (D_o = 1.8 mm, U = 1.8 m/s) for We = 135 and Re = 324. In order to evaluate the grid resolution effect, the height of the cylindrical column from droplet impingement up to jet breakup was examined. The crater formation after impact (region A), and Rayleigh jet before pinch-off and the recession of the jet back into the pool (region B), as well as the subsequent secondary droplet (region C) are shown in Fig. 3(a). It is clear that in region A, there is no significant variation in height for all cases. However, in regions B and C, grid independence was achieved for 10 μm × 10 μm, which is selected as the final grid.

D. Experimental validation of numerical results

The variation of the height of the cylindrical column up to the pinch-off was compared quantitatively with experimental

TABLE II. Information extracted from experiments using in-house developed MATLAB code for the same case shown in Fig. 5. ($t = 0$ is when the droplet contacts the pool surface.)

Event	Details
Droplet impact velocity	1.8 m/s
Evolution of crater depth	14 ms, from formation up to maximum depth
Critical height of Rayleigh jet	6.69 mm after $t = 42$ ms
Size of secondary droplet	1.45 mm diameter (pinch-off occurs at $t = 54$ ms)

results in Fig. 3(b). The numerical simulations were compared qualitatively with the experimental results in Fig. 4, where the secondary drop pinches off after 52.6 ms from the initial droplet impact. The results from the computational fluid dynamics (CFD) simulation match well with the experimental results. The errors in the maximum height of the jet and secondary droplet diameter were 2.2% and 3.4%, respectively. Videos S1 and S2 (see the Supplemental Material [42]) show the Rayleigh jet pinch-off and formation of two secondary droplets for silicone oil 5 cSt.

The CFD model predicted the critical Weber number for combinations of liquid properties and droplet diameter that led to Ohnesorge numbers of 0.007, 0.014, 0.044, and 0.060. In order to find out the transition boundaries between the jet formation and its breakup with subsequent formation of secondary drops, different impact velocities were tested. Nearly 30 numerical simulations, supplemented by 50 experiments (run three times for each We-Oh combination for repeatability) were carried out. A high-performance computing cluster was used to run all simulations.

IV. RESULTS AND DISCUSSION

A. Image processing results

The sequences of stages, registered by the high-speed camera, involve the initial droplet impact, crater formation, central (Rayleigh) jet evolution, subsequent jet breakup, and pinch-off of the secondary drops. In order to analyze the images more efficiently, a MATLAB code was developed for image processing. This code converts the gray scale images into binary and allows for extraction of impact characteristics mentioned earlier. The proper calibration factor is employed to convert pixel to millimeter [43]. Figure 5 shows four binary images from MATLAB, which are used to track the variation of the central column in time. These images correspond to silicone oil 5 cSt, $D_o = 1.8$ mm, and $U = 1.8$ m/s (Table II).

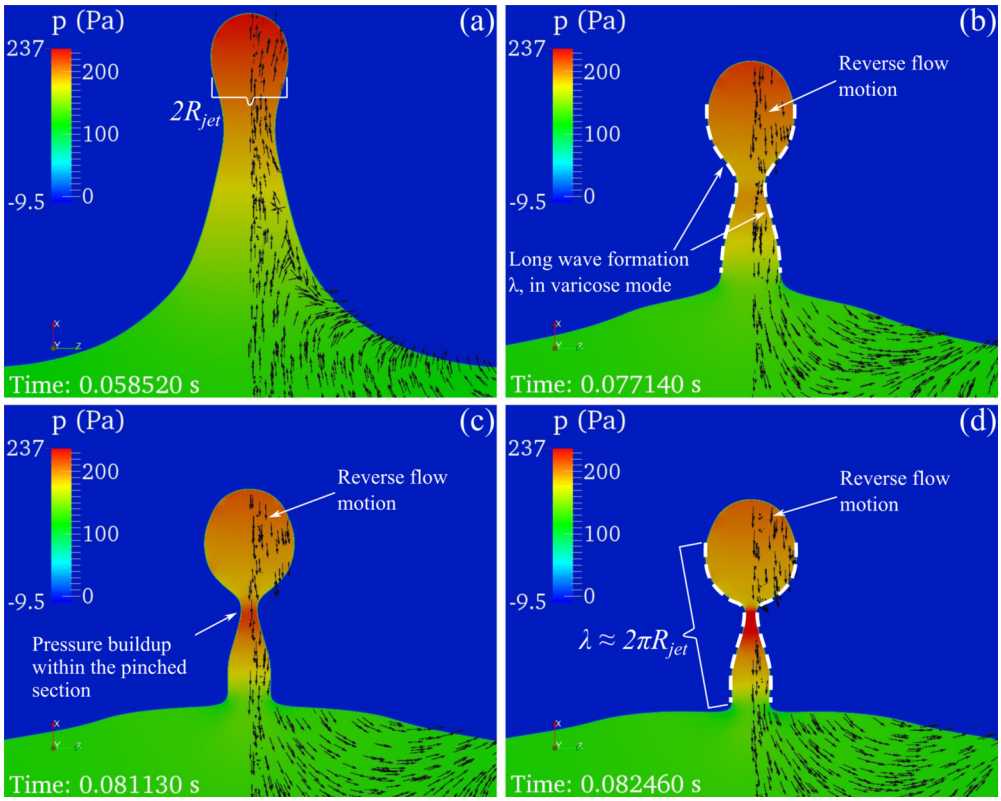

FIG. 6. (Color online) Pressure buildup in the pinched region after the impact of a silicone oil 1.8-mm droplet (10 cSt) with impact velocity of 2.5 m/s (We = 261, Oh = 0.0716). Pressure field is shown on each image and velocity vectors of the central Rayleigh jet are shown on the right side of each image. Some vectors have been removed for clarity.

TABLE III. Time scales of the problem sorted based on the Ohnesorge number (fluids).

Liquids	Oh	$t_{breakup}$(ms)	t_{cap}(ms)	t_{visc}(ms)
Water	0.0033	22.7	5.21	0.02
Potassium hydroxide	0.0033	18.0	5.94	0.02
Silicone oil 1 cSt	0.0070	24.7	5.81	0.04
Ethanol	0.0085	28.7	5.68	0.05
Silicone oil 2 cSt	0.0140	27.0	5.81	0.08
Silicone oil 5 cSt	0.0360	30.0	5.81	0.21
Silicone oil 5 cSt	0.0440	28.0	3.99	0.18
Silicone oil 8 cSt	0.0600	35.0	5.80	0.35
Silicone oil 10 cSt	0.0716	36.0	5.81	0.42
Ethylene glycol	0.0815	38.7	5.54	0.45
Silicone oil 13 cSt	0.0907	65.5	6.32	0.57

B. Physics behind Rayleigh jet formation and breakup

When a droplet impacts the pool with high kinetic energy, the impact causes large disturbances to the pool which forms a deep crater followed by a Rayleigh jet. The Rayleigh jet has the potential to break up due to Rayleigh-Plateau instability, as shown in Fig. 6. The Rayleigh-Plateau instability occurs when surface waves begin to form under the influence of surface tension. When the surface waves are of varicose mode and are long waves, a pinched region forms on the jet as shown in Fig. 6(b). As the amplitude of the long wave ($\lambda = 2\pi R_{jet}$) begins to grow, pressure begins to build up within the pinched region as shown in Fig. 6(c). The jet breaks up once the growth rate peaks. It should be noted that the wavelength is approximately the circumference of the jet and the growth rate for a jet has a capillary time scale, $t_{cap} \sim \sqrt{\rho R_{jet}^3 / \sigma}$, where R_{jet} is the radius of the jet [44]. The current experiments suggested that R_{jet} is of the same order of magnitude as the initial radius of the droplet (R_o), therefore $t_{cap} \sim \sqrt{\rho R_o^3 / \sigma}$. The viscosity of the jet plays no significant role on the range of unstable wavelengths. However, at higher Oh, viscosity can slow down the growth rate of the unstable waves with a viscous time scale of $t_{visc} \sim \mu R_{jet}/\sigma$ [45]. Additionally, the ratio of t_{visc} to t_{cap} represents the Ohnesorge number. Therefore, Oh is an indicator of how much the breakup time has lagged. As is seen in Table III, that capillary time scale and breakup time are of the same order, even though the former is approximately 3 to 10 times smaller than the latter. Thus, the capillary time scale is the appropriate scale to normalize breakup time. The breakup time is calculated from the time at which the jet emerges from the interface until it reaches the maximum height where it pinches off (Fig. 7). The nondimensional time, $t^*_{breakup}$, is seen to increase linearly with Oh up to Oh = 0.06, beyond which the curve becomes nonlinear.

Along with viscosity, the fluid motion of the jet can lag the breakup time as well. Since the emerging jet opposes gravity, the velocity of the jet reverses such that the fluid motion is directed towards the pool, as shown in Fig. 6. This reverse motion causes fluid to displace into the pinched section. While the velocity of the reverse fluid motion is not high enough to stabilize the jet, the reverse motion lags the breakup time. If the pinched section recedes back into the pool in a shorter time than the breakup time, breakup will not occur. Therefore there is a critical height that the jet must reach for breakup to occur. These critical heights are visualized in Fig. 8 and later quantified nondimensionally in Figs. 9 and 10.

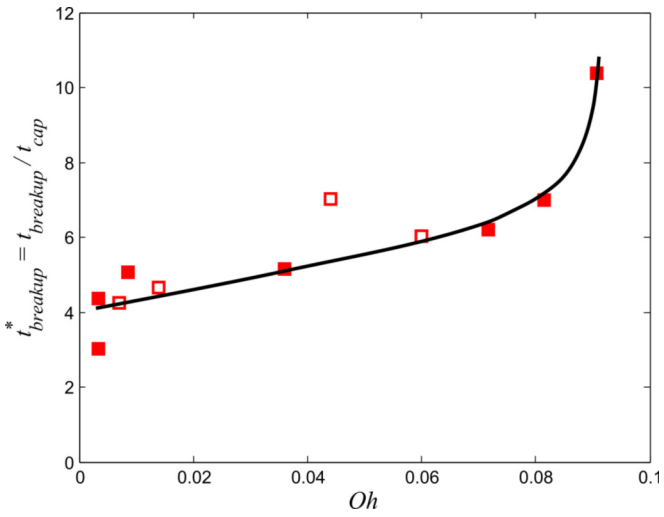

FIG. 7. (Color online) Normalized breakup time of the Rayleigh jet vs Ohnesorge number. The filled and unfilled symbols represent the experimental and numerical data, respectively.

In addition to the above phenomenon, it is observed that the reverse motion also occurs inside the droplet and the droplet has no distortion as the pinched section recedes back into the deep pool. The wavelength of the long wave does not significantly change while the amplitude grows. Therefore, the breakup of the pinched region is due to the Raleigh-Plateau instability caused by the temporal growth rate of the long wave. For partial coalescence to have occurred, the capillary waves would have traveled up the droplet causing the droplet to be distorted and pulled upward which leads to a pinch-off by stretching separation [21,33].

Typically, increase in impact velocity causes larger depth of crater and height of jet. It is also reasonable to conclude that the probability of jet breakup increases with impact velocity. Viscosity of the fluids tends to damp down the effect of the impact. For silicone oil 5 cSt, if $U = 1.8$ m/s (We = 135, Oh = 0.036), only one secondary drop was formed. At 2.1 m/s (We = 184), two secondary drops were formed, and at 2.3 m/s (We = 221) three secondary drops were formed (Fig. 8). Interestingly for silicone oil 20 cSt, even at velocities three times greater than critical impact velocity of silicone 5 cSt, no pinch-off was observed.

In the particular case shown in Fig. 8, where different numbers of secondary drops are formed, the secondary droplets display sizes of $0.58D_o$ to $0.94D_o$. It was observed that the size of secondary droplets varies for the different fluids and impact velocities that were tested in this study, but the order of magnitude for these drops remains the same as the mother droplet.

Among the cases that result in Rayleigh jet breakup and subsequent secondary droplet formation, the height of the Rayleigh jet was tracked up to the point where the first secondary droplet pinches off. Figure 9 depicts the variation of the normalized maximum height of Rayleigh jet as a function of impact We.

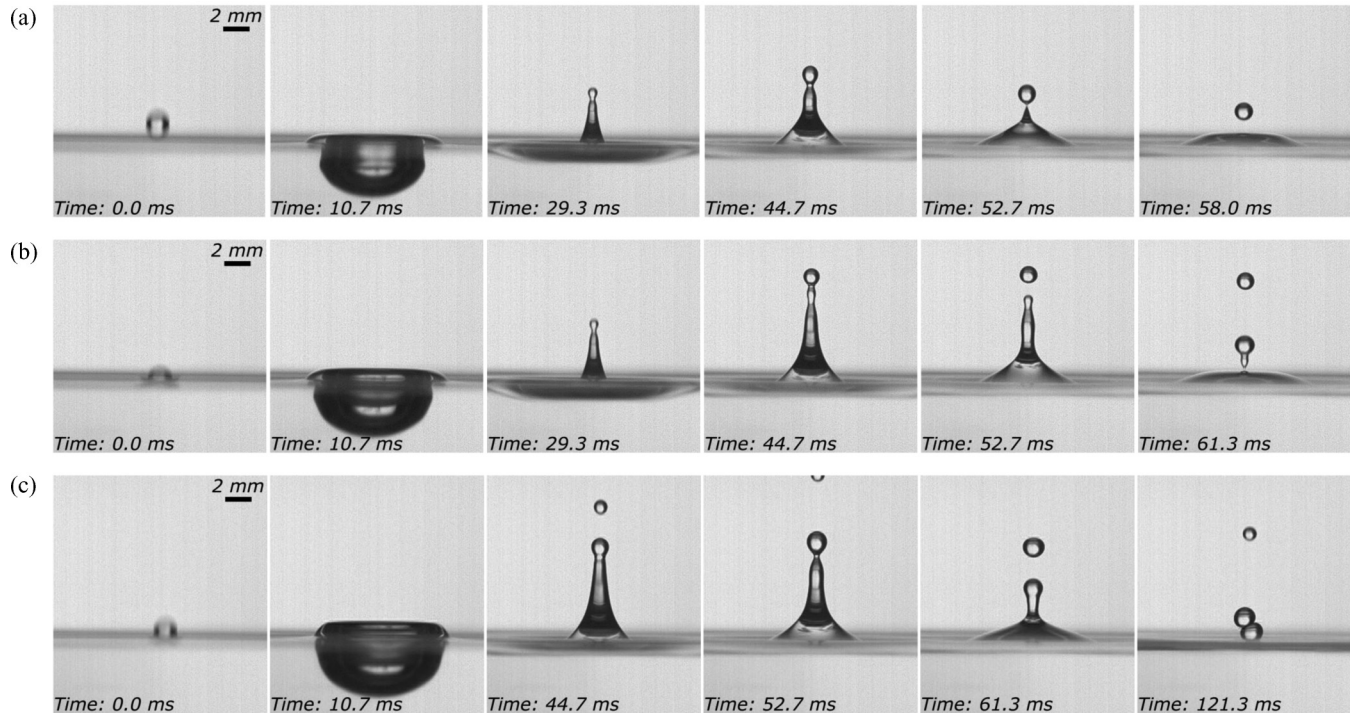

FIG. 8. Visualization of droplet impact process for a 5 cSt silicone oil drop at selected times for (a) $U = 1.8\,\mathrm{m/s}$ (We = 135), (b) $U = 2.1\,\mathrm{m/s}$ (We = 184), and (c) $U = 2.3\,\mathrm{m/s}$ (We = 221). All cases correspond to Oh = 0.036.

The higher the Ohnesorge number is, the lower the height of the Rayleigh jet. When Oh number increases, viscous forces become dominant over surface tension forces, which hinder the development of the jet as the capillary waves are not able to vertically stretch the droplet. The normalized height is also compared with its respective normalized time in Figs. 10(a) and 10(b). Properties of the liquid pool have an important role here. Higher Oh number tends to retard the evolution of the jet and subsequently the pinch-off process, in other words it takes longer time for the jet to reach a specific height compared to low Oh number fluids. It is noticeable that for silicone oil 13 cSt, which has the critical Ohnesorge number, the variation of maximum height of the jet with time is no longer linear. Moreover, Fig. 10(b) shows that there is a direct relationship between the nondimensional maximum height of the Rayleigh jet to form its first secondary droplet and the time associated with it. This relation is presented in Eq. (7), where $t^*_{h\,\mathrm{max}}$ is the normalized time required for the jet to reach its maximum height, and h^*_{max} is the normalized maximum height of the Rayleigh jet.

$$h^*_{\mathrm{max}} = 0.91 t^*_{h\,\mathrm{max}}. \tag{7}$$

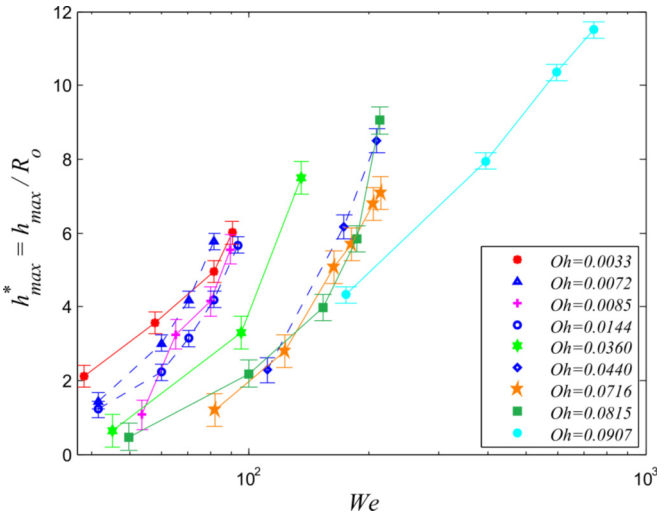

FIG. 9. (Color online) Normalized maximum height of the Rayleigh Jet, h^*_{max} up to the pinch-off of the first secondary drop vs impact Weber number, We.

Figure 11 demonstrates the evolution of cavity and the subsequent central jet for cases that show the Rayleigh jet breakup. The time is normalized with capillary time while the height of the jet and depth of penetration are normalized with droplet size. From Fig. 11(a) it can be seen that the depth of cavity at the time of jet eruption and pinch-off of first secondary drop decreases with Oh. In general, the fluids of lower viscosity show a deeper crater. This behavior was also observed by Ghabache *et al.* [31] in the jet formation from the bursting of a bubble. The evolution of the height of the central jet up to the pinch-off of the first secondary drop is shown in Fig 11(b). Indeed, the Oh number plays an important role in retarding the pinch-off process. By relating the dynamics of the cavity [Fig. 11(a)] to the height of the jet [Fig. 11(b)], it can be concluded that for higher Oh numbers (for fluids of higher viscosity), the effective size of the cavity is smaller. On the other hand, the critical height of the jet to pinch-off for fluids of higher viscosity is larger.

Figure 12 compares the shape of the crater for ethanol, silicone oil 5 cSt, and silicone oil 10 cSt. As observed by Ghabache *et al.* [31], it can also be noticed here that as viscosity

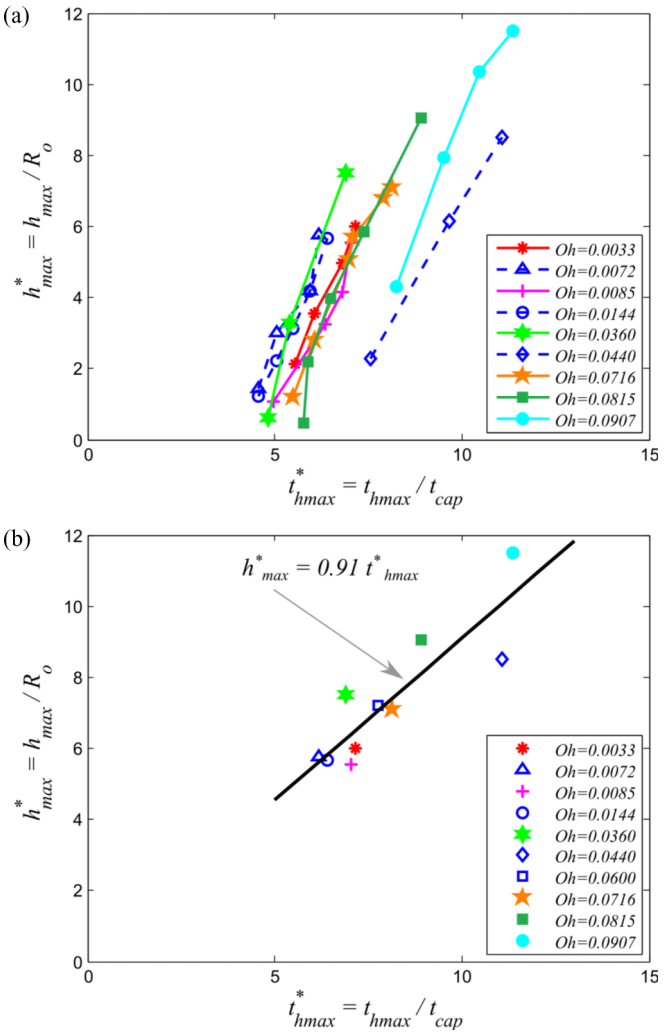

FIG. 10. (Color online) (a) Normalized maximum height of the Rayleigh jet up to the pinch-off of the first secondary drop vs normalized time, (b) Maximum height of Rayleigh jet for critical cases (at which pinch-off of the first secondary drop occurs) normalized by initial drop radius vs normalized time.

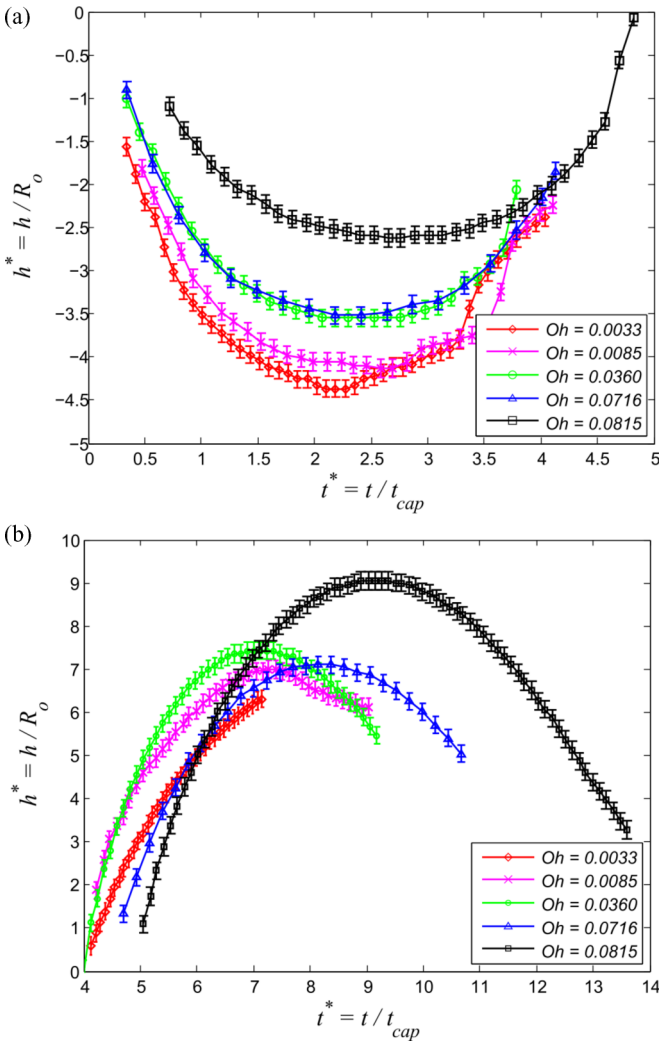

FIG. 11. (Color online) Tracking interface of (a) cavity and (b) central jet. The horizontal axis is normalized by capillary time and the vertical axis by initial droplet radius.

increases, the edges of the crater become smoother, particularly for silicone oil 10 cSt [Fig. 12(c)]. Figure 12(d) compares the overlap of collapsed cavity for the aforementioned fluids.

C. Effects of impact velocity, surface tension, and viscosity

The experiments were performed using distilled water, potassium hydroxide (KOH), ethanol, ethylene glycol, and silicone oils 5, 10, 13, 14, 16, 18, and 20 cSt, as summarized in Table I. The silicone oils have similar surface tension ($\sim$20 mN/m) and densities ($\sim$940 kg/m^3), but different viscosities. Except for water, the results were highly repeatable for the above-mentioned fluids. Water did not display consistent results under the same conditions, perhaps due to its impurities—an observation that was also made by others [46]. In order to confirm the water results, potassium hydroxide was tested since it has similar properties leading to the same Ohnesorge number as water (Table I). Among these fluids, the silicone oils showed the best repeatability at all stages, from the height of the Rayleigh jet to the number of secondary droplets at a certain impact Weber number.

The impact velocities were measured using image processing techniques and compared with $U = \sqrt{2gH}$ from conversion of potential energy into kinetic energy, where H is the release height. It is important to note that the values of U from experiments were always lower than that of theory, especially if the height exceeded 1 m. This is due to the drag force acting on the droplet. Therefore for consistency, the experimentally obtained impact velocities were used to calculate the nondimensional parameters shown in this study.

When a droplet impacts the pool of the same fluid, it penetrates through the interface and forms a crater. If the impact velocity is high enough, a central Rayleigh jet will form. Under certain conditions, the tip of the jet pinches off due to Rayleigh-Plateau instability and the secondary droplet forms. Many parameters can affect this behavior of which viscosity, surface tension, and impact velocity are the most important. The parameter of particular significance to identify the boundaries of transitions between no breakup and Rayleigh

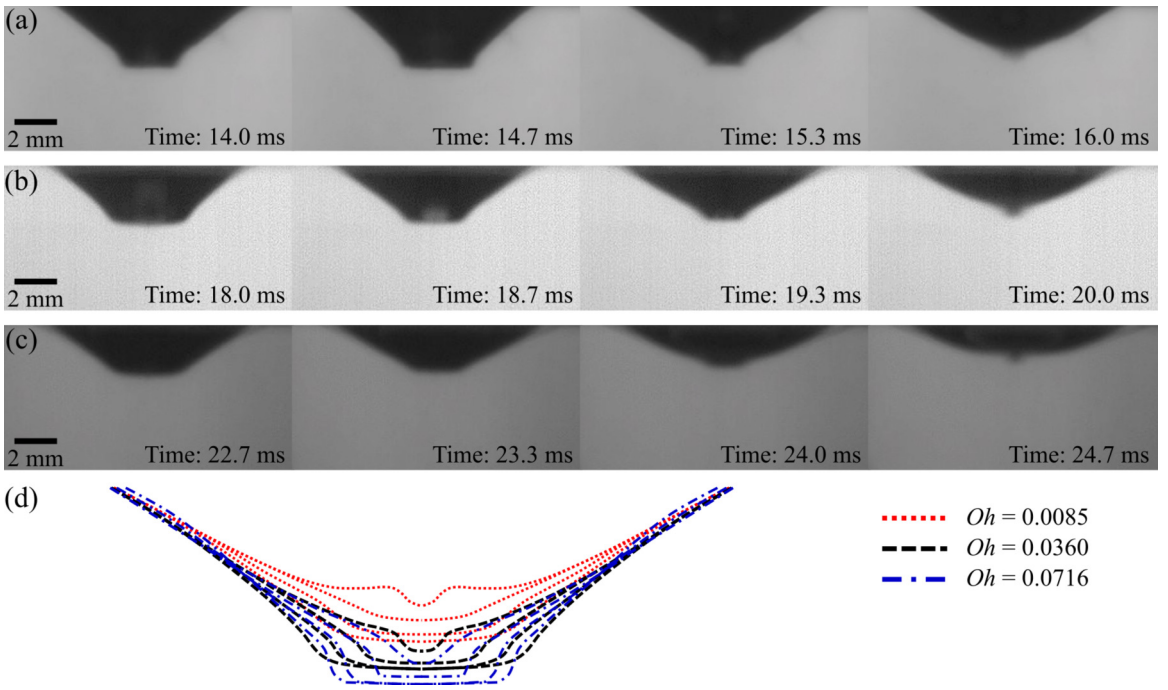

FIG. 12. (Color online) Dynamics of cavity for three fluids at selected times. (a–c) Depth of crater for ethanol, silicone oil 5 cSt, and silicone oil 10 cSt; (d) overlap of collapsed cavity for these fluids.

jet and later into crown splash is the Weber number. The impact Weber number where the jet breaks up and the secondary droplet forms is called the critical Weber number. When viscous effects are under consideration to study instability, Oh is a more appropriate parameter [47] as it isolates the property effects more. Re has also been used to classify the morphologies of crown droplets on a We-Re map [48]. In Figs. 13(a) and 13(b), regime maps for Rayleigh jet breakup,

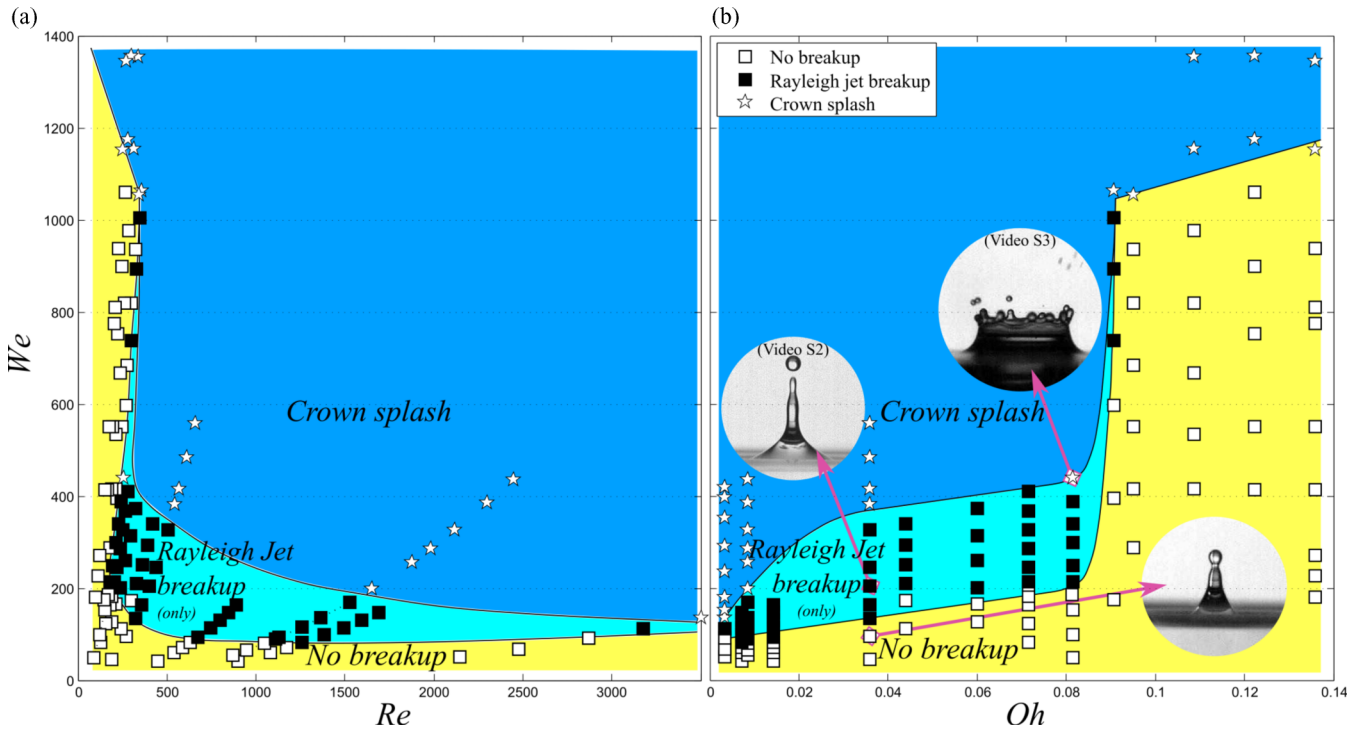

FIG. 13. (Color online) (a,b) Regime maps for Rayleigh jet breakup and subsequent secondary droplets formation based on Re and Oh, respectively. Filled markers represent the cases where breakup took place and single or multiple secondary droplets were observed. Blank and star symbols represent no breakup and crown splash, respectively. Ohnesorge numbers of 0.007, 0.014, 0.044, and 0.060 were obtained from numerical simulations. The rest of the cases were obtained from experimental results. Videos S2 and S3 can be found as Supplemental Material [42] representing each of these flow regimes both experimentally and numerically.

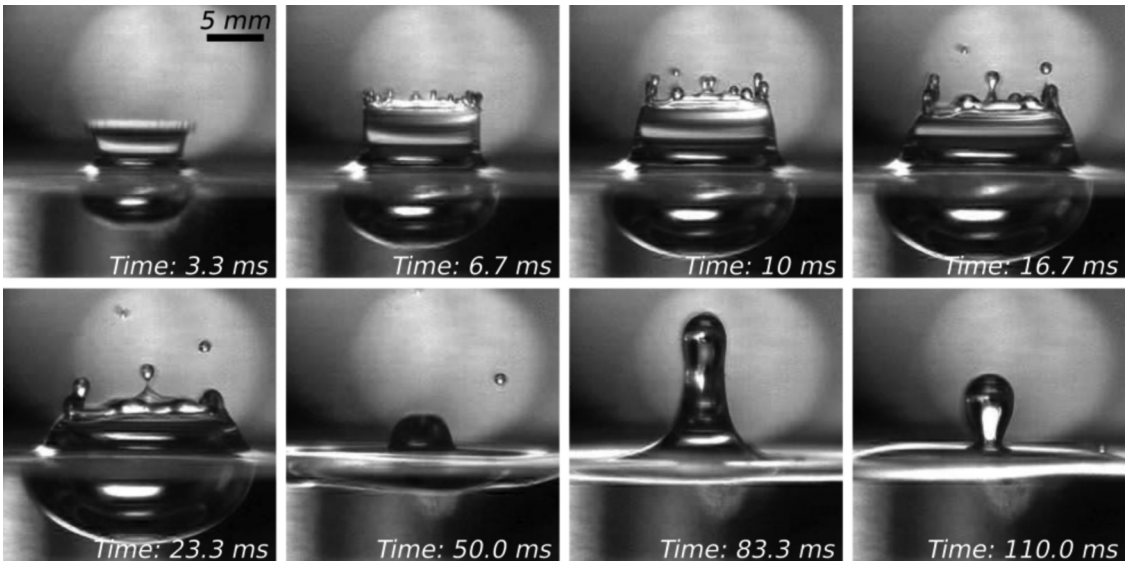

FIG. 14. Visualization of crown splash and Rayleigh jet formation for a silicone oil 20 cSt droplet impingement upon a pool of the same liquid. Re = 250, We = 1153, Oh = 0.1358. Time after initial droplet impact (D_o = 2.0 mm, U = 5.01 m/s) is shown in each snapshot.

crown splash, and subsequent formation of secondary droplets are plotted both as We vs Re and We vs Oh, respectively. Each Ohnesorge number represents a distinct fluid, whereas the variation in Weber number is due to changes in release height of the droplet.

For a combination of Oh $\leqslant$0.091 and Weber numbers beyond the critical value, the jet breakup leads to one or multiple secondary droplets that are on the order of $0.5D_o$ to $2D_o$. At low impact We number, the kinetic energy cannot overcome the surface tension forces. Depending on the impact velocity, in some cases, both Rayleigh jet breakup and crown splash can occur (Supplemental Material, video S3 [42]).

As viscosity increases, the kinetic energy at impact dissipates quicker, causing smaller disturbance to the pool, which decreases the height of the jet. In addition, the growth rate of Rayleigh-Plateau instability becomes smaller as viscosity increases [49]. Smaller growth rate further lags the breakup time. Therefore, for breakup to occur, the impact velocity or Weber number must increase as Oh number increases. However, if the Weber number increases high enough, the surface waves on the Rayleigh jet become short wave dominant. Short waves tend to stabilize the pressure fluctuations in the jet such that breakup does not occur [50]. Therefore there is a cutoff Oh at which Rayleigh-Plateau instability will no longer occur. From Fig. 13, it is observed that the cutoff Oh is $\approx$0.091. Existence of a critical Ohnesorge number is also confirmed by Blanchette and Bigioni [21], even though the size and impact velocity of droplets were not comparable with this study.

Interestingly, crown splash is observed to occur regardless of the cutoff Oh. Upon coalescence, the kinetic energy of the droplet is partially dissipated due to the viscous forces, the rest being transformed into surface energy distributed over a large surface area. At high impact velocities, the remainder of the kinetic energy results in the detachment of the lamellas from the liquid periphery. Typically, lower surface tension and viscosity combined with high impact velocity facilitate the crown formation. Viscosity is important since it determines the splash morphology. For high-viscosity fluids, the secondary drops detach only after the complete development of the crown but not in the early stages. However, for fluids with relative low viscosity, the crown splash can take place at early stages. The sequence of crown formation is presented in Fig. 14. Banks *et al.* studied the effect of viscosity on drop impacts onto thin films and delineated the crown behavior using the Weber number of the pool and the Ohnesorge number of the drop [47]. They have also confirmed that high viscosity could be a limit for the crown splashing phenomenon. Zhang *et al.* analyzed the wavelength selection and instabilities in the crown splash [48]; their findings support that Rayleigh-Plateau instability is the primary reason for secondary droplets.

V. CONCLUSIONS

In summary, the influence of fluid properties and impact velocity upon Rayleigh jet and pinch-off of secondary droplets have been studied for impact of a liquid droplet on a pool of identical fluid. To better understand the physical phenomena and confirm our observations, numerical simulations based on VOF and CSF methods were deployed. Increase in impact velocity (Weber number) increases the height of the thin column of fluid that emerges from the liquid pool. Under certain fluid conditions, the dissipation of this extra kinetic energy along with the surface tension forces produces instabilities in the neck of the jet. This could result in jet breakup and formation of secondary droplets. However, if the fluid has a high viscosity (i.e., high Ohnesorge number), a large portion of kinetic energy is dissipated; thus Rayleigh jet breakup may never occur. In other words, both the formation of the jet and its further breakup require a balance between viscous, capillary, and surface tension forces. A We-Oh plot shows three regimes for 0.0033 $\leqslant$ Oh $\leqslant$ 0.136. For Weber numbers beyond the critical value and Oh $\leqslant$ 0.091 the jet breakup occurs (Rayleigh jet breakup regime). While for Oh $>$ 0.091, the jet breakup is suppressed regardless of the

Weber number. In addition, high impact velocity initiates the crown formation and if further intensified it can disintegrate it into numerous secondary droplets. Since more viscous fluids tend to dampen the impact, they mitigate the occurrence of crown splash except at higher impact velocities. In addition, a correlation is proposed for normalized time with respect to the normalized maximum height of the jet.

ACKNOWLEDGMENTS

The authors would like to thank Dr. Carlos Velez for productive discussions on numerical simulations. We acknowledge University of Central Florida Advanced Research Computing Center (Stokes' Cluster) for providing required computational resources.

[1] B. Gopalan and J. Katz, Turbulent Shearing of Crude Oil Mixed with Dispersants Generates Long Microthreads and Microdroplets, Phys. Rev. Lett. **104**, 054501 (2010).

[2] A. M. Worthington, *A Study of Splashes* (Longmans, Green and Company, London, 1908), p. 129.

[3] J. C. Huang, A review of the state-of-the-art of oil spill fate/behavior models, in *International Oil Spill Conference Proceedings* (American Petroleum Institute, Washington, DC, 1983), Vol. 1983(1), p. 313.

[4] R. U. Meckenstock, F. von Netzer, C. Stumpp, T. Lueders, A. M. Himmelberg, N. Hertkorn, P. Schmitt-Kopplin, M. Harir, R. Hosein, S. Haque, and D. Schulze-Makuch, Water droplets in oil are microhabitats for microbial life, Science **345**, 673 (2014).

[5] S. D. Aziz and S. Chandra, Impact, recoil and splashing of molten metal droplets, Int. J. Heat Mass Transfer **43**, 2841 (2000).

[6] A. van der Bos, M. J. van der Meulen, T. Driessen, M. van der Berg, H. Reinten, H. Wijshoff, M. Versluis, and D. Lohse, Velocity Profile inside Piezoacoustic Inkjet Droplets in Flight: Comparison between Experiment and Numerical Simulation, Phys. Rev. Appl. **1**, 014004 (2014).

[7] T. Gilet and L. Bourouiba, Fluid fragmentation shapes rain-induced foliar disease transmission, J. R. Soc. Interface **12**, 20141092 (2015).

[8] S. Gart, J. E. Mates, C. M. Megaridis, and S. Jung, Droplet Impacting a Cantilever: A Leaf-Raindrop System, Phys. Rev. Appl. **3**, 044019 (2015).

[9] A. Davanlou and R. Kumar, Thermally induced collision of droplets in an immiscible outer fluid, Sci. Rep. **5**, 9531 (2015).

[10] A. Davanlou and R. Kumar, Counter-current motion of a droplet levitated on a liquid film undergoing Marangoni convection, Int. J. Heat Mass Transfer **89**, 345 (2015).

[11] A. L. Klein, W. Bouwhuis, C. W. Visser, H. Lhuissier, C. Sun, J. H. Snoeijer, E. Villermaux, D. Lohse, and H. Gelderblom, Drop Shaping by Laser-Pulse Impact, Phys. Rev. Appl. **3**, 044018 (2015).

[12] A. L. N. Moreira, A. S. Moita, and M. R. Panão, Advances and challenges in explaining fuel spray impingement: How much of single droplet impact research is useful? Prog. Energy Combust. **36**, 554 (2010).

[13] N. Laan, K. G. de Bruin, D. Bartolo, C. Josserand, and D. Bonn, Maximum Diameter of Impacting Liquid Droplets, Phys. Rev. Appl. **2**, 044018 (2014).

[14] C. Clanet, C. Béguin, D. Richard, and D. Quéré, Maximal deformation of an impacting drop, J. Fluid Mech. **517**, 199 (2004).

[15] R. Rioboo, C. Tropea, and M. Marengo, Outcomes from a drop impact on solid surfaces, Atom. Sprays **11**, 155 (2001).

[16] A. Gupta and R. Kumar, Two-dimensional lattice Boltzmann model for droplet impingement and breakup in low density ratio liquids, Commun. Comput. Phys. **10**(3), 767 (2011).

[17] M. Rein, Phenomena of liquid-drop impact on solid and liquid surfaces, Fluid Dyn. Res. **12**, 61 (1993).

[18] K. L. Pan and C. K. Law, Dynamics of droplet-film collision, J. Fluid Mech. **587**, 1 (2007).

[19] G. Agbaglah, M.-J. Thoraval, S. T. Thoroddsen, L. V. Zhang, K. Fezzaa, and R. D. Deegan, Drop impact into a deep pool: vortex shedding and jet formation, J. Fluid Mech. **764**, R1 (2015).

[20] A. Prosperetti and H. Oguz, The impact of drops on liquid surfaces and the underwater noise of rain, Annu. Rev. Fluid Mech. **25**, 577 (1993).

[21] F. Blanchette and T. P. Bigioni, Partial coalescence of drops at liquid interfaces, Nat. Phys. **2**, 254 (2006).

[22] T. Gilet, K. Mulleners, J. P. Lecomte, N. Vandewalle, and S. Dorbolo, Critical parameters for the partial coalescence of a droplet, Phys. Rev. E **75**, 036303 (2007).

[23] F. Blanchette, L. Messio, and J. W. M. Bush, The influence of surface tension gradients on drop coalescence, Phys. Fluids **21**, 072107 (2009).

[24] H. Aryafar and H. P. Kavehpour, Drop coalescence through planar surfaces, Phys. Fluids **18**, 072105 (2006).

[25] J. D. Paulsen, Approach and coalescence of liquid drops in air, Phys. Rev. E **88**, 063010 (2013).

[26] Z. Mohamed-Kassim and E. K. Longmire, Drop coalescence through a liquid/liquid interface, Phys. Fluids **16**, 2170 (2004).

[27] A. D. Bordoloi and E. K. Longmire, Effect of neighboring perturbations on drop coalescence at an interface, Phys. Fluids **24**, 062106 (2012).

[28] S.T. Thoroddsen and K. Takehara, The coalescence cascade of a drop, Phys. Fluids **12**, 1265 (2000).

[29] J. Hoepffner and G. Paré, Recoil of a liquid filament: escape from pinch-off through creation of a vortex ring, J. Fluid Mech. **734**, 183 (2013).

[30] P. Walls, L. Henaux, and J. Bird, Jet drops from bursting bubbles: How gravity and viscosity couple to inhibit droplet production, Phys. Rev. E **92**, 021002(R) (2015).

[31] E. Ghabache, A. Antkowiak, C. Josserand, and T. Séon, On the physics of fizziness: How bubble bursting controls droplets ejection, Phys. Fluids **26**, 121701 (2014).

[32] R. D. Deegan, P. Brunet, and J. Eggers, Complexities of splashing, Nonlinearity **21**, C1 (2008).

[33] X. Chen, S. Mandre, and J. J. Feng, Partial coalescence between a drop and a liquid-liquid interface, Phys. Fluids **18**, 051705 (2006).

[34] S. L. Manzello and J. C. Yang, An experimental study of a water droplet impinging on a liquid surface, Exp. Fluids **32**, 580 (2002).

[35] H. Aryafar and H. P. Kavehpour, Hydrodynamic instabilities of viscous coalescing droplets, Phys. Rev. E **78**, 037302 (2008).

[36] M. Rieber and R. Frohn, A numerical study on the mechanism of splashing, Int. J. Heat Fluid Flow **20**, 455 (1999).

[37] E. Berberović, N. P. van Hinsberg, S. Jakirlic, I. V. Roisman, and C. Tropea, Drop impact onto a liquid layer of finite thickness: Dynamics of the cavity evolution, Phys. Rev. E **79**, 036306 (2009).

[38] B. Ray, G. Biswas, and A. Sharma, Regimes during liquid drop impact on a liquid pool, J. Fluid Mech. **768**, 492 (2015).

[39] C. W. Hirt and B. D. Nichols, Volume of fluid (VOF) method for the dynamics of free boundaries, J. Comput. Phys. **39**, 201 (1981).

[40] J. U. Brackbill, D. B. Kothe, and C. Zemach, A continuum method for modeling surface tension, J. Comput. Phys. **100**, 335 (1992).

[41] H. G. Weller, A new approach to VOF-based interface capturing methods for incompressible and compressible flow, Report TR/HGW/04, OpenCFD Ltd, Bracknell, Berkshire, UK.

[42] See Supplemental Material at http://link.aps.org/supplemental/10.1103/PhysRevE.92.053022 for videos. Video S1: Numerical simulation of Rayleigh jet breakup and formation of two secondary droplets (silicone oil 5 cSt, Do = 1.8 mm, U = 2.1 m/s). Video S2: Experimental observation of Rayleigh jet breakup and formation of two secondary droplets (silicone oil 5 cSt, Do = 1.8 mm, U = 2.1 m/s). Video S3: Crown splash and subsequent Rayleigh jet breakup (ethylene glycol, Do = 2.2 mm, U = 4.16 m/s).

[43] A. Davanlou, Integration of fiber-optic sensors in measuring machines, Measurement **57**, 25 (2014).

[44] J. Eggers and E. Villermaux, Physics of liquid jets, Rep. Prog. Phys. **71**, 036601 (2008).

[45] P. Deepu, S. Basu, and R. Kumar, Dynamics and fracture of ligaments from a droplet on a vibrating surface, Phys. Fluids **25**, 082106 (2013).

[46] T. Tran, H. de Maleprade, C. Sun, and D. Lohse, Air entrainment during impact of droplets on liquid surfaces, J. Fluid Mech. **726**, R3 (2013).

[47] D. Banks, C. Ajawara, R. Sanchez, H. Surti, and G. Aguilar, Effects of drop and film viscosity on drop impacts onto thin films, Atom. Sprays **23**(6), 555 (2013).

[48] L. V. Zhang, P. Burnet, J. Eggers, and R. D. Deegan, Wavelength selection in the crown splash, Phys. Fluids **22**, 122105 (2010).

[49] S. Chandrasekhar, *Hydrodynamic and Hydromagnetic Stability* (Oxford University Press, New York, 1961).

[50] L. E. Johns and R. Narayanan, *Interfacial Instability* (Springer, New York, 2002).